ChemComm

COMMUNICATION

View Article Online
View Journal | View Issue

Cite this: *Chem. Commun.*, 2017, 53, 12438

Received 25th September 2017,
Accepted 27th October 2017

DOI: 10.1039/c7cc07465d

rsc.li/chemcomm

Chemical antagonism between photodynamic agents and chemotherapeutics: mechanism and avoidance†

Qingshuo Meng,‡[ab] Jia Meng,‡[ab] Wei Ran,[ab] Jinghan Su,[ab] Yuguang Yang,[c] Pengcheng Zhang *[ab] and Yaping Li *[ab]

We report a photochemical reaction-induced antagonism between the photodynamic agent (PS) and anti-cancer drugs during combined therapy. The annihilation of singlet oxygen and alkene-containing drugs into inactive drug hydroperoxides is responsible for the antagonism, and results in decreased efficacy against several cancer cell lines. Experimental and simulation results reveal that the annihilation abates with increasing distance between the PS and drugs *via* confining the PS and drugs into separated vehicles. As a result, antagonism can be switched to synergism in treating both drug sensitive and resistant cancer cells.

Photosensitizers (PSs) have shown great potential in photocatalysis and cancer therapy due to their capability to conduct light-powered chemical reactions.[1–4] Given their controllable and potent activity, PS-based nanoparticles have served as both drugs and carriers, which include titanium dioxide,[5] plasmonic vesicles,[6,7] upconversion nanoparticles,[8] gold nanorods,[9] PS-conjugated antibodies,[10] porphysomes,[11,12] and PS-loaded liposomes.[13,14] However, the treatment effect induced by PSs is transient and is also limited by the depth of tissue penetration of the laser, which hampers the application of PS-based therapy.[15] Many efforts have been devoted to developing PSs with absorbance in the second near-infrared window, as lasers in this range show high tissue penetration.[16] An alternative and effective strategy to address this issue is combination therapy, exemplified by nanoparticles with both chemotherapy and photodynamic therapy (PDT) activities.[13,17–27] These nanoparticles are effective for cancer therapy because localized singlet oxygen ($^1O_2$) or reactive oxygen species (ROS) produced by the PS can facilitate extravasation and tissue penetration of chemotherapeutics *via* triggering the apoptosis of both cancerous and endothelial cells.[28–30] Also, the short-lived $^1O_2$ or ROS can control the release of chemotherapeutics enveloped by carriers and subcellular vesicles to realize long-term inhibition of tumor growth and metastasis.[13,17–22] However, the same strategy would also generate, in nanoparticles, a high local concentration of $^1O_2$/ROS that are reactive to drugs in the same carrier. The interaction between the PS and drugs during the treatments is largely unclear, in contrast to tremendous efforts and successes in the development of such nanoparticles for combination therapy. So far, only a few studies have reported pharmacologic or pharmacokinetic antagonism between PDT and chemotherapy.[31,32] It is crucial to understand the photochemistry behind the interactions between PS generated $^1O_2$ and drugs before clinical translation of these nanomedicines.[33]

In this communication, we report a chemical antagonism between the PS chlorin e6 trimethyl ester (Ce6tM) and chemotherapeutics (Fig. 1a). Drugs of different structures, including curcumin (polyphenol), docetaxel (taxane), mertansine (maytansinoid), vinorelbine (vinca alkaloids), and rapamycin (macrolide) were used as model drugs (Fig. 1b), among which the latter four are being used or tested in the clinic for cancer therapy. Regardless of their different structures, they were all deposited together with Ce6tM in the lipid bilayers (~5 nm in thickness) of vesicles (60–70 nm in diameter) formed by dipalmitoyl-*sn*-glycero-3-phosphocholine (DPPC) (dual-drug loaded liposomes, DL-X), revealed by cryogenic transmission electron microscopy (cryo-TEM) and confocal laser scanning microscopy (CLSM) (Fig. S1 and S2, ESI†). The hydrodynamic size of the vesicles (~80 nm) determined by dynamic light scattering (DLS) was consistent with that determined by cryo-TEM (Table S1, ESI†). Quantitative encapsulation of Ce6tM and drugs also suggested preferential drug accumulation in the hydrophobic membrane of the vesicles (Tables S2 and S3, ESI†). Mono-drug loaded liposomes (ML-X) containing either Ce6tM or drug were prepared, and were similar to DL-X in morphology and size (Fig. S3 and Tables S1–S3, ESI†). These results revealed that Ce6tM and drugs were concentrated in the membrane of the vesicles.

The close deposition of Ce6tM and drugs in the lipid bilayer of the vesicles would enable possible chemical reactions. We,

[a] *State Key Laboratory of Drug Research & Center of Pharmaceutics, Shanghai Institute of Materia Medica, Chinese Academy of Sciences, 501 Haike Road, Shanghai 201203, China. E-mail: pzhang@simm.ac.cn, ypli@simm.ac.cn*
[b] *University of Chinese Academy of Sciences, 19 Yuquan Road, Beijing 100049, China*
[c] *Department of Chemical and Biomolecular Engineering, Johns Hopkins University, 3400 North Charles Street, MD 21218, USA*

† Electronic supplementary information (ESI) available. See DOI: 10.1039/c7cc07465d
‡ These authors contributed equally to this work.

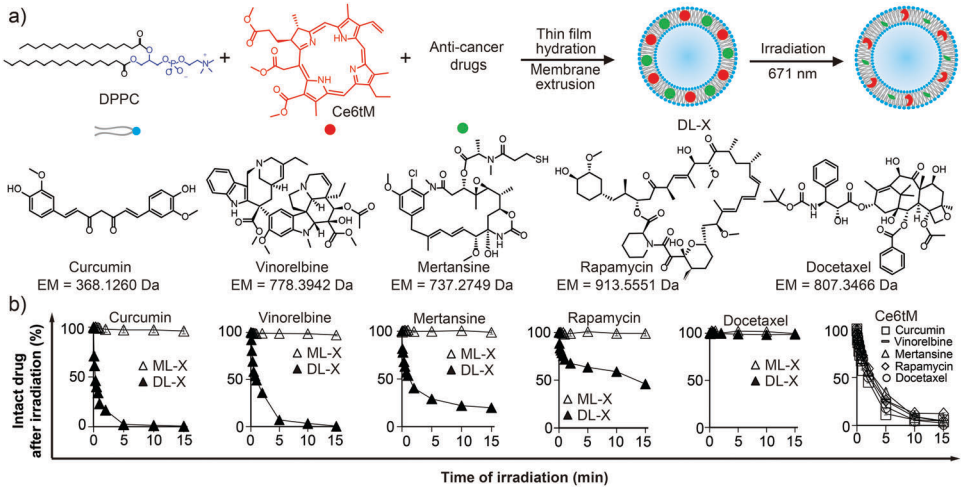

Fig. 1 Preparation and irradiation-induced drug decomposition of DL-X. (a) Schematic illustration of the preparation and irradiation-induced drug decomposition in DL-X. The chemical structures and their exact mass (EM) were listed. (b) Time-dependent degradation of anti-cancer drugs and Ce6tM in different vesicles under laser irradiation (671 nm, 2 W cm^{-2}). The initial concentrations of Ce6tM and anti-cancer drugs were 235 and 118 μM, respectively.

therefore, irradiated the liposomes with a 671 nm laser and monitored their changes using multiple techniques. We first observed a dramatic change (colored to colorless) in the color of DL-X (Fig. S4, ESI†). The qualitative observation suggested that both the drugs and PS degraded during irradiation (Fig. 1a), which urged us to perform a quantitative study. Fig. 1b shows the degradation profiles of anti-cancer drugs in DL-X and ML-X under laser irradiation using high-performance liquid chromatography (HPLC). The rates of drug decomposition varied for different DL-X, with 76%, 51%, 46%, 22%, 0.3% and ~30–40% of curcumin, vinorelbine, mertansine, rapamycin, docetaxel, and Ce6tM decomposed within 1 min, respectively. Drug decomposition accelerated when the amount of Ce6tM relative to drug increased (Table S4, ESI†) or when higher irradiation power was applied to the solutions (Fig. S5, ESI†). These results demonstrated the existence of chemical antagonism between PDT and chemotherapy. Though fast and dramatic drug and Ce6tM decomposition was recorded, cryo-TEM imaging and DLS analysis revealed no obvious change in the morphology, size, size distribution, surface charge and bilayer structure of DL-X before and after irradiation, or when compared with ML-X (Fig. S6, S7 and Table S1, ESI†).

We then explored the mechanism that led to the chemical antagonism. It turned out that $^1O_2$ was the dominant if not the only factor driving the process, as significant and fast $^1O_2$ production was detected using an SOSG-based method (SOSG is a $^1O_2$ activatable fluorescent probe) in DL-SOSG but not ML-SOSG (Fig. 2a). Synchronized $^1O_2$ production and drug decomposition was always observed under conditions of varying Ce6tM-to-drug ratios and irradiation powers (Fig. S5, S8, S9 and Table S4, ESI†). When $^1O_2$ was quenched by 30 mM sodium azide (NaN_3, a scavenger of $^1O_2$[34]) (Fig. S10, ESI†), degradation of the drugs in DL-X was also prohibited (Fig. 2b). All these results confirmed the pivotal role of $^1O_2$ in the observed chemical antagonism.

It has been reported that $^1O_2$ can react with biomacromolecules and alkene-containing chemicals to generate hydroperoxides whose

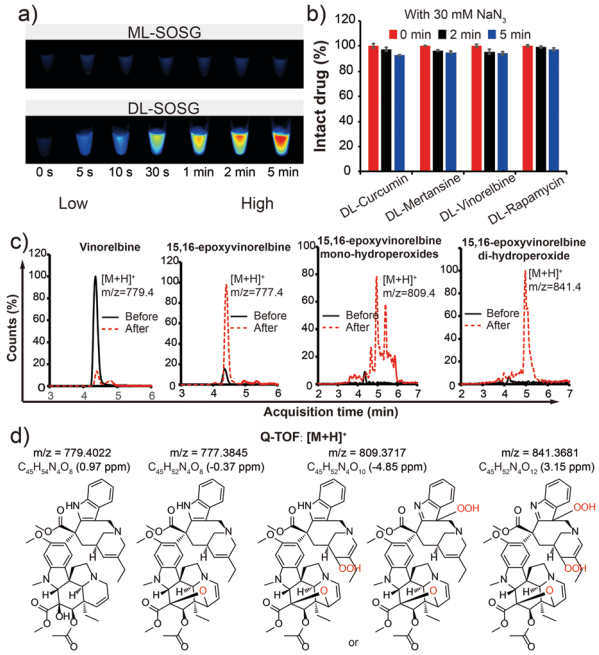

Fig. 2 The mechanism of photo-induced drug decomposition. (a) Fluorescence images of irradiated ML-SOSG and DL-SOSG solutions (Epi illumination: 455–485 nm, emission filter: 530/28 nm). (b) Anti-cancer drugs remained intact in co-delivery liposomes in the presence of 30 mM NaN_3. (c) LC-MS spectrum of DL-vinorelbin before and after irradiation. (d) The exact mass of generated species and the most plausible formulas (mass accuracy) and structures.

exact masses are ~32*n* Da (*n* = 1, 2, 3, *etc.*) larger than those of the parental molecules.[35,36] We, therefore, monitored the mass change using liquid chromatography–mass spectrometry (LC-MS). In irradiated DL-vinorelbine, we observed a dramatic conversion of vinorelbine to species whose exact masses were 2.0 Da less or 30.0 and 62.0 Da larger than that of vinorelbine (Fig. 2c). Further quad-time-of-flight (Q-TOF) LC-MS-MS analysis revealed that the 2.0177 Da mass loss was due to the deprivation of 2 hydrogen atoms associated with the formation of 15,16-epoxyvinorelbine

(a major metabolite of vinorelbine[37]) (Fig. 2d). The 31.9872 and 63.9846 Da mass increase from that of 15,16-epoxyvinorelbine suggested the addition of 2 and 4 oxygen atoms (Fig. 2d). There were two possible mono-hydroperoxide isomers of different retention times in the LC-MS spectrum. However, we were unable to assign the peaks to the corresponding isomers, as each captured fragment could not be exclusively associated with one reaction site (Fig. S11, ESI†). Similar studies were performed on other DL-X, and the results strongly indicated that curcumin, mertansine-Pyr (use instead of mertansine, EM = 846.2735 Da) and rapamycin were all converted into the corresponding hydroperoxides (Fig. S12–S14, ESI†), while no drug conversion was observed in DL-docetaxel (Fig. S15, ESI†). To investigate the exact structures of the hydroperoxides, techniques such as nuclear magnetic resonance (NMR) will be required. Unfortunately, due to their reactivity, the purification of hydroperoxides would be challenging, and it might be necessary to develop suitable online NMR reaction monitoring technologies.[38]

The $^1O_2$, while decomposing drugs, was simultaneously quenched by them. We compared the release of $^1O_2$ from DL-X relative to ML-Ce6tM, using SOSG-based fluorometry. We found that DL-X released significantly less $^1O_2$ than ML-Ce6tM ($p < 0.0005$), and the more susceptible a co-encapsulated drug to $^1O_2$, the less $^1O_2$ released from the corresponding DL-X (Fig. S16, ESI†). Since $^1O_2$ was the executor of PDT, the result here suggested that co-delivered chemotherapeutics could also antagonize the efficacy of PDT.

Given the great potential of combined PDT and chemotherapy in cancer management,[13,39] it is necessary to develop a strategy that allows simultaneous use of the two modalities with minimized annihilation. One possible strategy is placing drugs some distance (l) away from the PS (Fig. 3a) so that short-lived $^1O_2$ (lifespan = 3.5 ms[40]) could destroy cancer cells before annihilating with drugs. To test our hypothesis, the rates of drug decomposition in DL-X and physical mixtures of ML-X and ML-Ce6tM were compared. Reduced drug degradation was observed when l = 488 nm (0.6 mg mL^{-1} in DPPC) (Fig. 3b) but not when l = 157 nm (18 mg mL^{-1} in DPPC) (Fig. S17, ESI†). Meanwhile, no such big difference was observed for DL-X under the same concentrations. To understand the observed phenomenon, we estimated the mean first collision time (MFCT) of liposomes under Brownian motion (the detailed method is provided in the ESI†). The collision was defined when $l < 90$ nm (the nearest distance between Ce6tM and anti-cancer drug molecules would be shorter than 20 nm[40]). The MFCTs of liposomes under the two conditions were 473 ± 74 and 12.5 ± 1.7 μs (15626 liposomes each experiment, average from 200 experiments for each condition), respectively, indicating a more frequent collision of liposomes in concentrated solution. We simulated the random walks of 216 liposomes (2 types mixed at a 1 : 1 ratio) under the two conditions (Movies S1 and S2, ESI†), and ~50-fold faster collision of liposomes was recorded in concentrated solution (Fig. 3c). These results proved that using a physical mixture instead of DL-X could be a feasible and effective strategy to mitigate the antagonism between PS and drugs.

We finally evaluated the *in vitro* activity of vinorelbine-loaded liposomes against human A549 non-small cell lung cancer cells, B16-F10 melanoma cancer cells, HT29 colon cancer cells, and MCF-7 breast cancer cells, after confirming that only marginal drug release

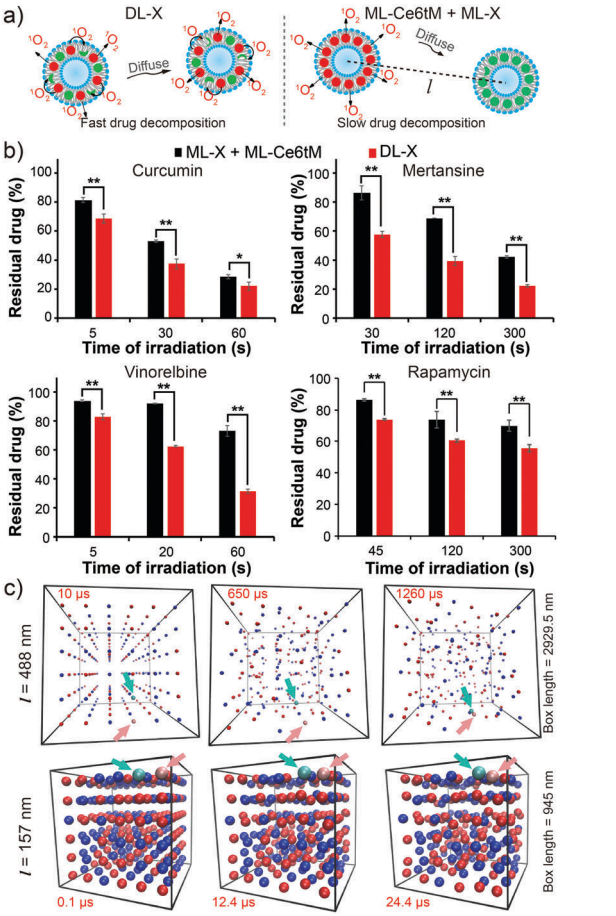

Fig. 3 Effect of distance between the PS and drugs on chemical antagonism. (a) Schematical illustration of the effect of distance between the PS and drugs on drug decomposition. (b) The comparison of drug decomposition rates in DL-X and a corresponding mixture of ML-X and ML-Ce6tM. (c) Snapshots of 216 liposomes (red: ML-Ce6tM; blue: ML-X) before 2 of them (light red and light blue ones, indicated by arrows) collided. The data were represented as mean ± s.d. (n = 3). *$p < 0.05$, **$p < 0.005$.

within 8 h of incubation (Table S5, ESI†). We first investigated the effect of hydroperoxide formation on vinorelbine activity and found that the two were negatively correlated (Table S6, ESI†), indicating that hydroperoxides of vinorelbine are not active. Similar results were observed from the formulations of the remaining three drugs on the 4 cell lines (Tables S7–S9, ESI†). We further evaluated the synergistic effect of combined therapies on A549 and MCF-7, as well as their drug resistant strains (A549T and MCF-7/ADR, about 20- and 7-fold more resistant to vinorelbine than the parental cell lines, respectively, Table S10, ESI†). Hydroperoxides of vinorelbine were much less active and unable to kill >50% of the resistant cells under 30 μg mL^{-1} (Table S10, ESI†). After confirming the resistance, the cells were irradiated after a 4 h incubation period. On drug resistant cell lines, the IC50 of DL-vinorelbine was ~1.5-fold that of ML-Ce6tM (Fig. 4). In sharp contrast, the physical mixture (ML-vinorelbine + ML-Ce6tM) was ~5-fold more effective than ML-Ce6tM, while ML-vinorelbine alone was ineffective under the same conditions (Fig. 4). A similar trend was observed on drug sensitive A549 and MCF-7 cells (Fig. S18, ESI†). These results proved the existence of antagonism between closely deposited PS and drugs. The antagonism effect is

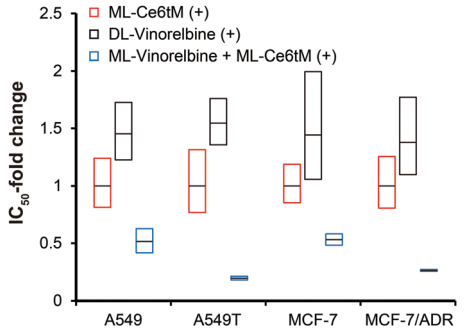

Fig. 4 Change in the IC_{50} of vinorelbine-containing formulations relative to ML-Ce6tM. Boxes show 95% confidence ranges with the median in black.

rooted in the chemical susceptibility of drugs and the consequent annihilation of $^1O_2$ and alkene-containing drugs (Fig. 3a and Fig. S16, ESI†). The rate of annihilation will drop dramatically in the presence of steric hindrance near the alkene group,[41] which may cause the ultra-slow degradation of docetaxel (Fig. 1). These results also demonstrated that a profound synergistic effect could be achieved using a physical mixture strategy, probably due to an enhanced cytosol delivery of chemotherapeutics during PDT.[13,14,17–24,30,42] Since the combined use of PDT and other treatments is among the fastest growing fields of nano-medicine,[43] we believe that the knowledge acquired herein would facilitate the rational design and development of new and powerful combined nano-therapeutics.

In conclusion, we have reported the chemical antagonism between Ce6tM and drugs, which could be generalize to any generator of $^1O_2$ and therapeutics (small molecules, proteins/peptides, and nucleotides[35,36,44]) containing susceptible moieties such as phenol, indole, or alkene groups. More importantly, we have shown that the chemical antagonism could be addressed by encapsulating the two modalities into separated liposomes. The findings here highlight that chemical compatibility of combined drugs, in addition to compatibilities in their mechanism of action and pharmacokinetic properties, should be taken into consideration when designing new combined therapies.

This work was financially supported by the National Natural Science Foundation of China (81521005, 81270047, and 81671808) and the Youth Innovation Promotion Association of CAS (2017335). We are grateful to the National Centre for Protein Science Shanghai (Electron Microscopy system) for their instrument support and technical assistance.

Conflicts of interest

There are no conflicts to declare.

Notes and references

1 W. J. Youngblood, S. H. Lee, K. Maeda and T. E. Mallouk, *Acc. Chem. Res.*, 2009, **42**, 1966–1973.
2 P. Wu, C. He, J. Wang, X. Peng, X. Li, Y. An and C. Duan, *J. Am. Chem. Soc.*, 2012, **134**, 14991–14999.
3 M. Ethirajan, Y. Chen, P. Joshi and R. K. Pandey, *Chem. Soc. Rev.*, 2011, **40**, 340–362.
4 J. F. Lovell, T. W. Liu, J. Chen and G. Zheng, *Chem. Rev.*, 2010, **110**, 2839–2857.
5 N. Kotagiri, G. P. Sudlow, W. J. Akers and S. Achilefu, *Nat. Nanotechnol.*, 2015, **10**, 370–379.
6 J. Song, P. Huang, H. Duan and X. Chen, *Acc. Chem. Res.*, 2015, **48**, 2506–2515.
7 J. Lin, S. Wang, P. Huang, Z. Wang, S. Chen, G. Niu, W. Li, J. He, D. Cui, G. Lu, X. Chen and Z. Nie, *ACS Nano*, 2013, **7**, 5320–5329.
8 N. M. Idris, M. K. Gnanasammandhan, J. Zhang, P. C. Ho, R. Mahendran and Y. Zhang, *Nat. Med.*, 2012, **18**, 1580–1585.
9 J. Conde, N. Oliva, Y. Zhang and N. Artzi, *Nat. Mater.*, 2016, **15**, 1128–1138.
10 M. Mitsunaga, M. Ogawa, N. Kosaka, L. T. Rosenblum, P. L. Choyke and H. Kobayashi, *Nat. Med.*, 2011, **17**, 1685–1691.
11 J. F. Lovell, C. S. Jin, E. Huynh, H. Jin, C. Kim, J. L. Rubinstein, W. C. Chan, W. Cao, L. V. Wang and G. Zheng, *Nat. Mater.*, 2011, **10**, 324–332.
12 E. Huynh, B. Y. Leung, B. L. Helfield, M. Shakiba, J. A. Gandier, C. S. Jin, E. R. Master, B. C. Wilson, D. E. Goertz and G. Zheng, *Nat. Nanotechnol.*, 2015, **10**, 325–332.
13 B. Q. Spring, R. Bryan Sears, L. Z. Zheng, Z. Mai, R. Watanabe, M. E. Sherwood, D. A. Schoenfeld, B. W. Pogue, S. P. Pereira, E. Villa and T. Hasan, *Nat. Nanotechnol.*, 2016, **11**, 378–387.
14 A. Y. Rwei, J. J. Lee, C. Zhan, Q. Liu, M. T. Ok, S. A. Shankarappa, R. Langer and D. S. Kohane, *Proc. Natl. Acad. Sci. U. S. A.*, 2015, **112**, 15719–15724.
15 P. Zhang, C. Hu, W. Ran, J. Meng, Q. Yin and Y. Li, *Theranostics*, 2016, **6**, 948–968.
16 G. Hong, A. L. Antaris and H. Dai, *Nat. Biomed. Eng.*, 2017, **1**, 0010.
17 C. He, D. Liu and W. Lin, *ACS Nano*, 2015, **9**, 991–1003.
18 C. He, X. Duan, N. Guo, C. Chan, C. Poon, R. R. Weichselbaum and W. Lin, *Nat. Commun.*, 2016, **7**, 12499.
19 D. Luo, N. Li, K. A. Carter, C. Lin, J. Geng, S. Shao, W. C. Huang, Y. Qin, G. E. Atilla-Gokcumen and J. F. Lovell, *Small*, 2016, **12**, 3039–3047.
20 D. Luo, K. A. Carter, A. Razi, J. Geng, S. Shao, D. Giraldo, U. Sunar, J. Ortega and J. F. Lovell, *Biomaterials*, 2016, **75**, 193–202.
21 Y. Yuan, J. Liu and B. Liu, *Angew. Chem., Int. Ed.*, 2014, **53**, 7163–7168.
22 T. T. Wang, D. G. Wang, H. J. Yu, M. W. Wang, J. P. Liu, B. Feng, F. Y. Zhou, Q. Yin, Z. W. Zhang, Y. Z. Huang and Y. P. Li, *ACS Nano*, 2016, **10**, 3496–3508.
23 C. Wang, X. Sun, L. Cheng, S. Yin, G. Yang, Y. Li and Z. Liu, *Adv. Mater.*, 2014, **26**, 4794–4802.
24 Q. Chen, X. Wang, C. Wang, L. Z. Feng, Y. G. Li and Z. Liu, *ACS Nano*, 2015, **9**, 5223–5233.
25 L. Feng, L. Cheng, Z. Dong, D. Tao, T. E. Barnhart, W. Cai, M. Chen and Z. Liu, *ACS Nano*, 2017, **11**, 927–937.
26 Y. Wang, Y. Xie, J. Li, Z. H. Peng, Y. Sheinin, J. Zhou and D. Oupicky, *ACS Nano*, 2017, **11**, 2227–2238.
27 Y. Li, Y. Deng, X. Tian, H. Ke, M. Guo, A. Zhu, T. Yang, Z. Guo, Z. Ge, X. Yang and H. Chen, *ACS Nano*, 2015, **9**, 9626–9637.
28 I. Rizvi, J. P. Celli, C. L. Evans, A. O. Abu-Yousif, A. Muzikansky, B. W. Pogue, D. Finkelstein and T. Hasan, *Cancer Res.*, 2010, **70**, 9319–9328.
29 B. W. Henderson and T. J. Dougherty, *Photochem. Photobiol.*, 1992, **55**, 145–157.
30 D. Luo, K. A. Carter, A. Razi, J. Geng, S. Shao, C. Lin, J. Ortega and J. F. Lovell, *J. Controlled Release*, 2015, **220**, 484–494.
31 E. Crescenzi, A. Chiaviello, G. Canti, E. Reddi, B. M. Veneziani and G. Palumbo, *Mol. Cancer Ther.*, 2006, **5**, 776–785.
32 M. F. Zuluaga and N. Lange, *Curr. Med. Chem.*, 2008, **15**, 1655–1673.
33 K. Glusac, *Nat. Chem.*, 2016, **8**, 734–735.
34 T. Maisch, J. Baier, B. Franz, M. Maier, M. Landthaler, R. M. Szeimies and W. Baumler, *Proc. Natl. Acad. Sci. U. S. A.*, 2007, **104**, 7223–7228.
35 M. J. Davies, *Biochem. Biophys. Res. Commun.*, 2003, **305**, 761–770.
36 M. Prein and W. Adam, *Angew. Chem., Int. Ed. Engl.*, 1996, **35**, 477–494.
37 K. Yamaguchi, T. Yasuzawa, T. Sakai and S. Kobayashi, *Xenobiotica*, 1998, **28**, 281–291.
38 D. A. Foley, E. Bez, A. Codina, K. L. Colson, M. Fey, R. Krull, D. Piroli, M. T. Zell and B. L. Marquez, *Anal. Chem.*, 2014, **86**, 12008–12013.
39 S. W. Morton, M. J. Lee, Z. J. Deng, E. C. Dreaden, E. Siouve, K. E. Shopsowitz, N. J. Shah, M. B. Yaffe and P. T. Hammond, *Sci. Signaling*, 2014, **7**, ra44.
40 S. Hatz, J. D. Lambert and P. R. Ogilby, *Photochem. Photobiol. Sci.*, 2007, **6**, 1106–1116.
41 C. W. Jefford and A. F. Boschung, *Helv. Chim. Acta*, 1974, **57**, 2242–2257.
42 J. G. Shiah, Y. G. Sun, C. M. Peterson, R. C. Straight and J. Kopecek, *Clin. Cancer Res.*, 2000, **6**, 1008–1015.
43 L. Cheng, C. Wang, L. Feng, K. Yang and Z. Liu, *Chem. Rev.*, 2014, **114**, 10869–10939.
44 S.-j. Park, W. Park and K. Na, *Adv. Funct. Mater.*, 2015, **25**, 3472–3482.